Proton radiation damage study of the next generation of swept charge devices

Conference or Workshop Item

Proton Radiation Damage Study of the Next Generation of Swept Charge Devices

J. Gow*[a], A. D. Holland[a], P. Pool[b]

[a]e2v centre for electronic imaging, The Open University, PSSRI, Milton Keynes, MK7 6AA, UK
[b]e2v technologies plc, 106 Waterhouse Lance, Chelmsford, Essex, CM1 2QU, UK

ABSTRACT

The first generation of Swept Charge Device (SCD) the e2v technologies plc CCD54 was used in the Demonstration of a Compact Imaging X-ray Spectrometer (D-CIXS) launched in 2003 and again in the Chandrayaan-1 X-ray Spectrometer (C1XS) instrument currently in orbit around the Moon. The main source of decreased energy resolution in both cases is proton damage, from trapped and solar protons respectively. This paper presents the results from an experimental study to evaluate the performance of the next generation of SCD the CCD234 and CCD236 irradiated with a 10 MeV equivalent proton fluence of 3.0×10^{8} protons.cm^{-2}, demonstrating the factor of two increase in radiation hardness when compared to the CCD54. In particular the increased dark current, decrease in energy resolution and the degradation of charge transfer efficiency (CTE) are described.

Keywords: Swept Charge Device, SCD, proton radiation damage, charge transfer efficiency, displacement damage hardened

1. INTRODUCTION

The work presented in this paper has been carried by the e2v centre for electronic imaging at the Open University to investigate the post proton irradiation performance of the second generation of Swept Charge Devices (SCDs) the CCD234 and CCD236. The CCD234, produced by e2v technologies plc, is based on the heritage of the CCD54 launched onboard Chandrayaan-1 in 2008 as part of the Chandrayaan-1 X-ray Spectrometer (C1XS) instrument [Howe *et al.* 2009], a descendant of the Demonstration of a Compact Imaging X-ray Spectrometer (D-CIXS) instrument flown onboard SMART-1 launched in 2003 [Grande *et al.* 2003]. The CCD234, illustrated in Figure 1(a), has an active area of ~1.1 cm^2 comparable with the active are of the CCD54. Unlike the CCD54 the CCD234 only uses one central transfer channel to reduce the volume in which charge is transported to provide improved radiation hardness through improved charge transfer. It also makes use of a dummy output adjacent to the output node to enable suppression of clock-induced pickup from the video signal. The CCD236, illustrated in Figure 1(b), is essentially four CCD234s in a four leaf clover design with an active area of ~4.2 cm^2, the signals from the four quadrants are combined before the readout node.

a) b)

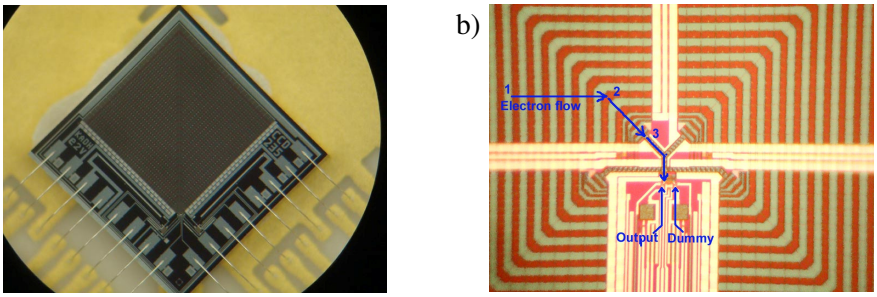

Fig. 1. A photograph of the CCD234 (a) and the output area of the CCD236 (b) showing the two phase image clocks, the outputs and the electron flow [Holland 2007]

*jpdg3@open.ac.uk; phone +44 (0) 1908 852 769; fax +44 (0) 1908 858 052; www.open.ac.uk/cei

The SCD was developed by e2v technologies to perform as an X-ray spectrometer in the energy range 0.5-10.0 keV, the CCD234 achieves near Fano-limited spectroscopy at -10 °C. The herringbone electrode structure of the CCD54 shown in Figure 2(a) which used a 3-phase clocking operation has been replaced with the perpendicular structure illustrated in Figure 2(b), and a 2-phase clocking operation to facilitate charge transfer in a large 'pixel'. The simpler clocking operation and increased pixel size allow to device to be readout in a shorter time improving the temporal resolution and allowing device size to be increased. The electrodes are indicated by the dashed lines and the charge transport channels by the solid lines. The pitch of the channel stops has been increased from 25 μm to 100 μm for improved charge collection within one 'sample'. Due to the non-imaging readout of the SCD where charge is swept continuously towards the readout node, producing a linear readout of 'samples'. The concept of a 'pixel' is not strictly applicable, though charge moves through 'charge transfer elements' whose structure is the same as a pixel. The SCD readout is referred to as samples.

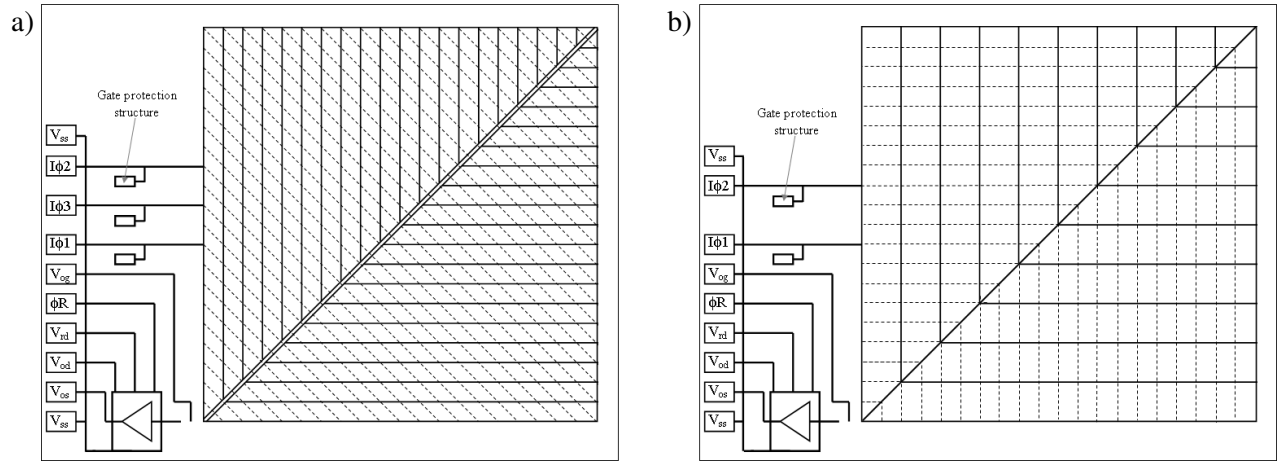

Fig. 2. Schematic of the CCD54 (a) and the CCD234 (b), indicating the various clocks and biases required

A proton irradiation study was conducted using one CCD234 and one CCD236 with the irradiation carried out at the Kernfysisch Versneller Instituut (KVI) in the Netherlands. A 10 MeV equivalent proton fluence of 3.0×10^{8} protons.cm^{-2} was selected as the target fluence to allow a comparison with the CCD54, irradiated as part of the Chandrayaan-1 radiation damage study [Gow et al. 2008]. The key aims were to asses the radiation tolerance of the second generation SCDs in comparison to the first, looking at energy resolution, noise, dark current, percentage of isolated events and the main source of performance loss as a function of temperature, charge transfer inefficiency (CTI) or bulk dark current (inverted devices limit the contribution from surface generated dark current). In general CTI is measured as a 'per transfer' number, however the total loss is dependant on the volume of silicon through which charge is transferred, rather than how many clock cycles are used. In this report CTI refers to the total charge lost across the device and not as a function of the number of transfers required to readout the device [Gow and Holland 2009].

2. EXPERIMENTAL ARRANGEMENT

The CCD234 package includes a thermo-electric cooler (TEC) and a Fenwal thermistor to allow the device temperature to be monitored, the CCD236 was mounted onto an aluminium cold finger attached to a one stage TEC with a 1000 Ω platinum resistance thermometer fitted to the invar base to monitor temperature. Temperature control to ±0.1 °C was provided by an ILX Lightwave controller (model number LDT-5525). The SCD device being tested was housed inside a vacuum test facility, illustrated in Figure 3, mounted on a copper heat exchanger through which water flowed removing the heat from the back of the TEC. An Oxford Instruments X-ray tube was used to provide secondary Cu-Kα X-rays from a copper target held at 45° to the incident X-rays. SCD drive electronics were provided by Xcam Ltd. and the data were recorded on a laptop computer.

A drive sequence was used to readout the whole device area, resetting the charge packet for each subsequent sample. Only isolated events were used in the analysis presented in this report, found using code designed in MatLab with a threshold of two times the standard deviation of the noise peak. Each device was tested between 10 °C and -35 °C with data acquired using three sets of 600 device readouts for the CCD234 and 2000 device readouts for the CCD236, both devices were operated at 120 kHz. The operating voltages for the CCD234 and CCD236 are given in Table 1, at this time the performance has not been optimised and used values from pre-irradiation testing. The characterisation of the CCD54 is discussed in Gow 2008.

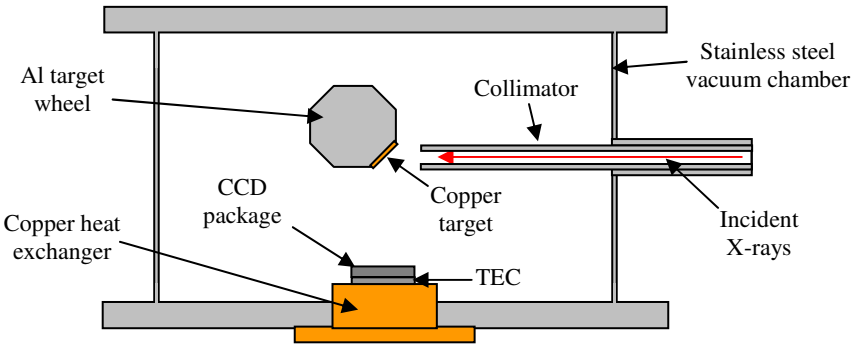

Fig. 2. Schematic of the SCD test facility

Table 1. SCD operational voltages

Parameter	***Range***	***Typical (V)***
V_{ss}	8.5 – 10 V	9.0
V_{og}	2 – 5 V	3.0
V_{rd}	15 – 20 V	17.0
V_{od}	29 – 32 V	30.0
IØ	6 – 12 V	7.7
ØR1	5 - 11 V	7.0
DD	Not critical	20.0

2.1 Proton Irradiation

The irradiation was performed successfully at KVI. The beam energy was measured to be 44 MeV at the CCD, irradiating the whole active area of the CCD234 and CCD236. The 10 MeV equivalent proton fluence delivered to each device was 3.0×10^{8} protons.cm^{-2} delivered over a period of 67 seconds, the irradiation details are given in Table 2. The field uniformity was measured using a LANEX (Kodak) scintillating screen, and found to be ±10% in dose over an area 70-80mm [van de Graff 2008]. Over 10.5 mm the beam is uniform to ±3%.

Table 2. Irradiation Characteristics for the CCD234 and CCD236

Parameter	***Value***
Beam Energy	44 MeV
Beam Fluence	5.4×10^{8} p.cm^{-2}
Beam Flux	8.1×10^{6} p.cm^{-2}.s^{-1}
Exposure Time	67 s
Equivalent 10 MeV Fluence	**3.0×10^{8} p.cm^{-2}**
Beam diameter	8 cm
Beam uniformity	10% over ϕ8cm 3% over central ϕ1 cm

3. RESULTS AND DISCUSSIONS

3.1 Dark Current Performance

Due to the readout nature of the SCD there is no dark current reference level, to find the system noise reference level the device was cooled to remove dark current contribution, providing the system noise. The total noise includes the system and read noise components, the dark current can then be estimated subtracting the square of the system noise from the total measured noise. The results for the CCD54 [Gow and Holland 2009] and CCD234 are shown in Figure 3 and for the CCD234 and CCD236 in Figure 4, values have been normalised to a readout rate of 100 kHz to be comparable with the readout rate of the CCD54. Dark current is dependant on the area and readout rate, not on the number of clock cycles. As would be expected of similar sized devices Figure 4 demonstrates that the CCD54 and CCD234 have a similar dark current profile as a function of temperature, with dark current increasing accordingly post irradiation. The four times higher dark current of the CCD236 shown in Figure 4 is as a result of the four times larger detector area. As a function of area the increase in dark current of the CCD234 and CCD236 is exactly in keeping with that of the CCD54.

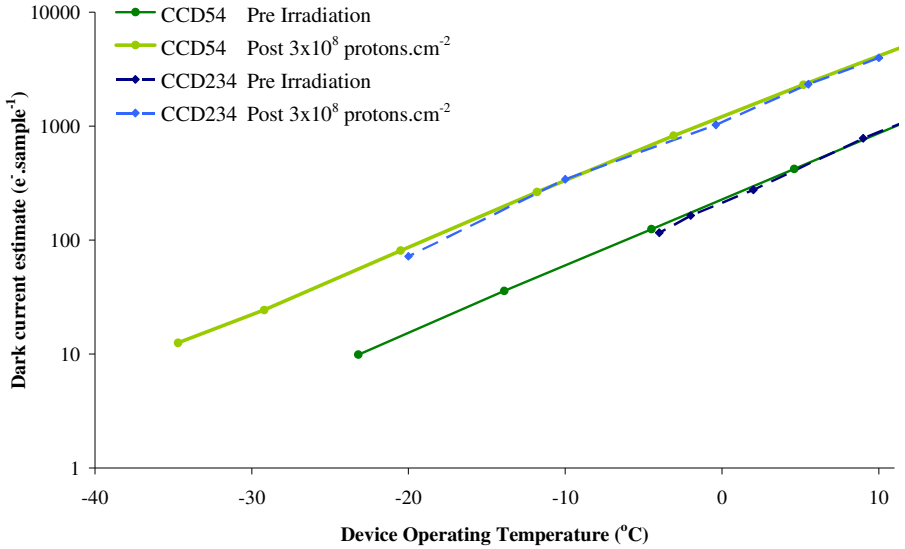

Fig. 3. Dark current of the CCD54 and CCD234 pre and post irradiation as a function of temperature

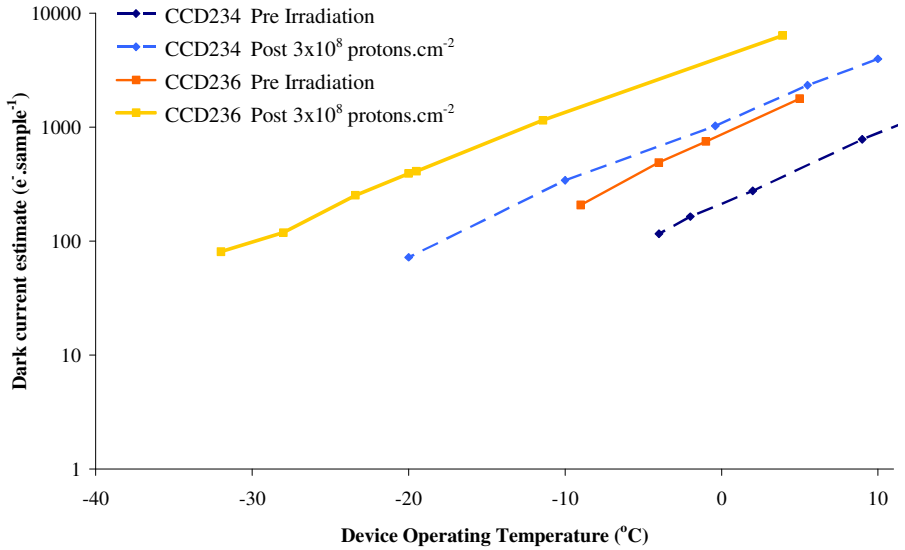

Fig. 4. Dark current of the CCD234 and CCD236 pre and post irradiation as a function of temperature

3.2 X-ray Detection

The ability to collect all the charge generated by an X-ray event within one sample is essential to provide a high energy resolution, the CCD54 started to exhibit poor charge collection at ~3.6 keV, i.e. less than 50% isolated sample events. An isolated event is defined as an event where the adjacent samples have an ADC value less than a threshold of two times the standard deviation of the noise peak. The pixel pitch of the CCD54 was 25 µm using a 3-phase clocking operation (30% under potential for collection) whereas the pixel pitch of the new SCDs is 4 times larger at 100 µm using a 2-phase clocking operation (50% under potential for collection) resulting in a significantly higher number of X-rays detected as isolated events. Table 3 provides the typical event splitting frequency measured to within ± 1% of the CCD54, CCD234 and CCD236 post irradiation with the pre irradiation values of the CCD54 and CCD236 given in brackets. The 100 µm pitch allows 71% of the high energy Cu-Kα X-ray events at 8.047 keV to be detected within one sample, while only 44% were collected in the CDD54. The small change experienced post irradiation can be attributed to statistical variations on the measurements, and the slight increase in dark current non-uniformity.

Table 3. Typical event size frequencies for Cu-Kα events post irradiation and in brackets those values pre-irradiation

Event Size (samples)	***Typical Frequency (%)***		
	CCD234	CCD236	CCD54
1	71 (72)	72 (71)	44 (44)
2	28 (27)	27 (26)	38 (35)
3	1 (1)	1 (3)	8 (9)

3.3 X-ray Spectroscopy Performance

The pre irradiation energy resolution at Cu-Kα of the CCD234 is comparable with the CCD54 below -10 °C, the higher energy resolution of the CCD234 above -10 °C is as a result of the lower dark current generated by operating at 120 kHz compared to the CCD54 operated at 100 kHz. Post irradiation with a 10 MeV equivalent proton fluence of 3.0 x10^8 protons.cm^{-2} the decrease in energy resolution exhibited by the CCD54 at -28 °C, where dark current is minimised, is over twice that exhibited by the CC234, illustrated in Figure 5. Pre-irradiation the higher dark current generated in the CCD236 limits the measured energy resolution, the device requires further cooling to achieve comparable results to the CCD234, as shown in Figure 6. Accounting for the difference in size pre-irradiation performance is similar. At -30 °C the CCD236 provides improved post irradiation performance when compared to the CCD54.

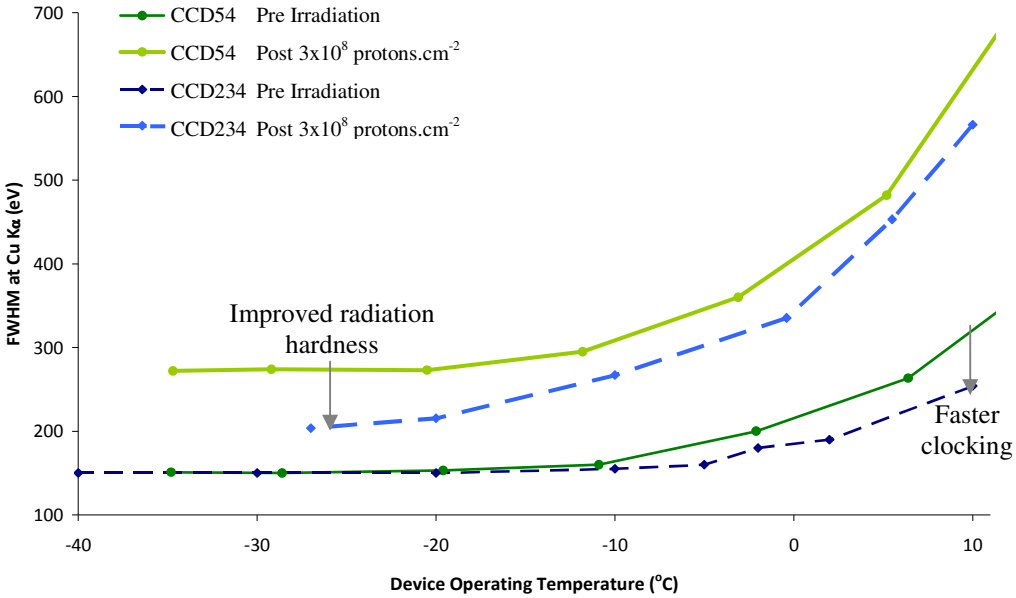

Fig. 5. Energy resolution of isolated Cu-Kα events found using the CCD54 and CCD234 pre and post irradiation as a function of temperature

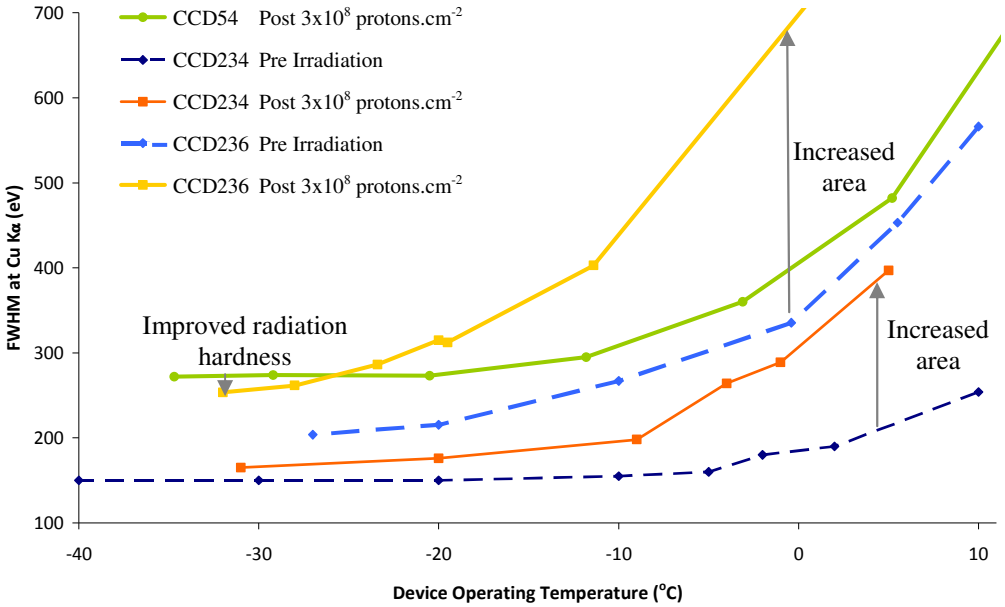

Fig. 6. Energy resolution of isolated Cu-Kα events found using the CCD54 post irradiation, and the CCD234 and CCD236 pre and post irradiation as a function of temperature

It has been shown that the pre irradiation energy resolution were in very good agreement with the predicted energy resolution based on the quadrature summation of the X-ray Fano-limited statistics (FE/ω) plus the measured total noise (σ) to give a predicted FWHM for both the CCD236 [Holland 2007] and the CCD54 [Gow *et al.* 2008]. This means that pre-irradiation the CTI of these devices is not affecting the device performance to within the limits of the measurement technique, as shown in Figures 7, 8 and 9 which show the predicted energy resolution and the measured energy resolution as a function of temperature of the CCD54, CCD234 and CCD236 respectively. The effect of thresholding was ruled out by reducing the threshold until there was no longer any change in the measured energy resolution.

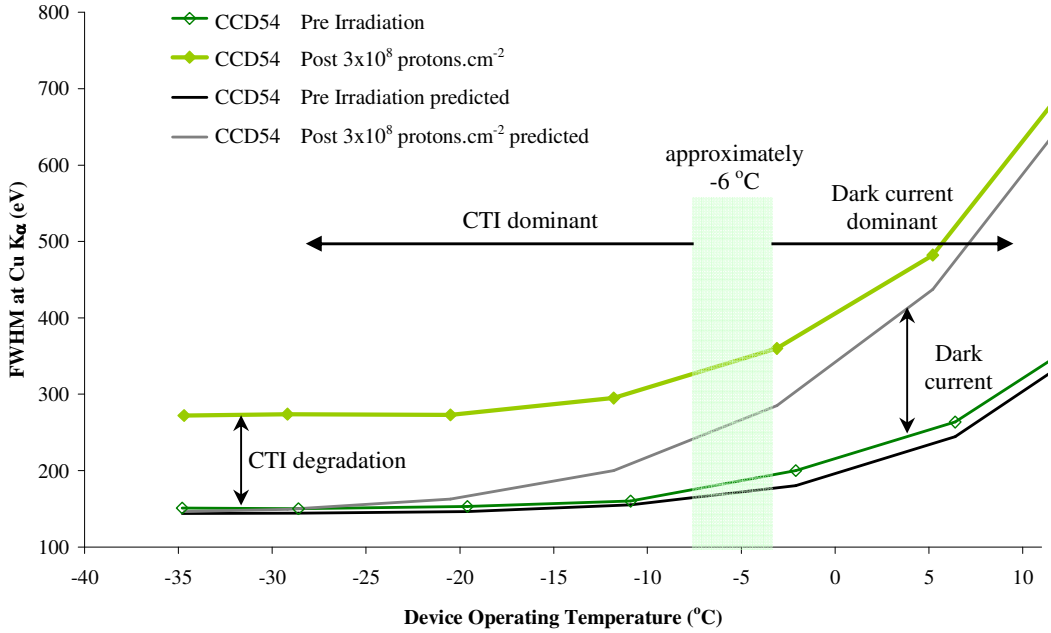

Fig. 7. Measured and predicted (based on noise and Fano factor) energy resolution of isolated Cu-Kα events found using the CCD54 pre and post irradiation as a function of temperature

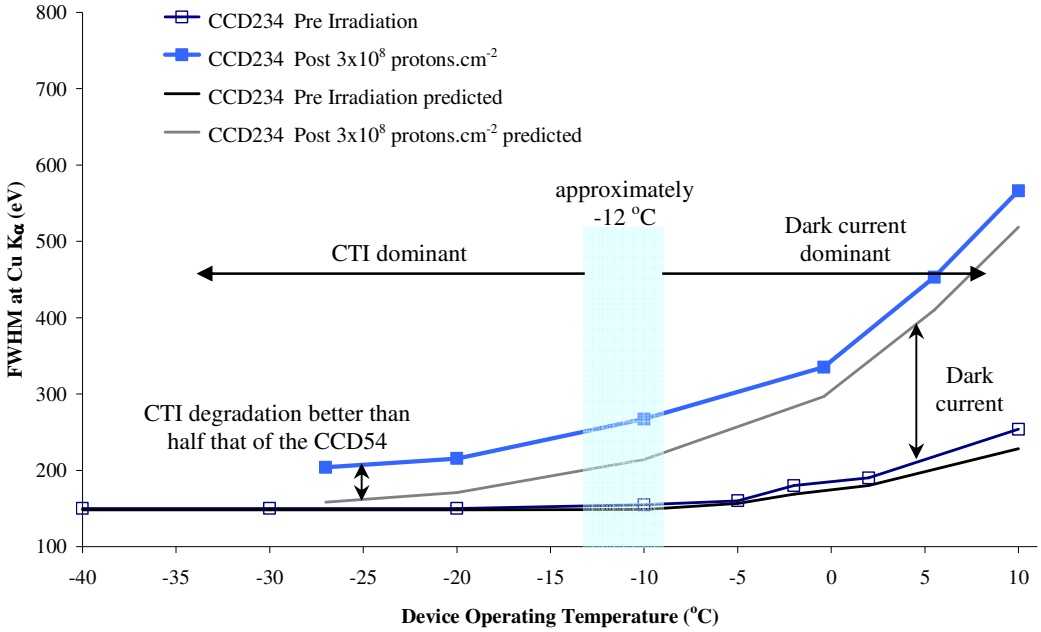

Fig. 8. Measured and predicted (based on noise and Fano factor) energy resolution of isolated Cu-Kα events found using the CCD234 pre and post irradiation as a function of temperature

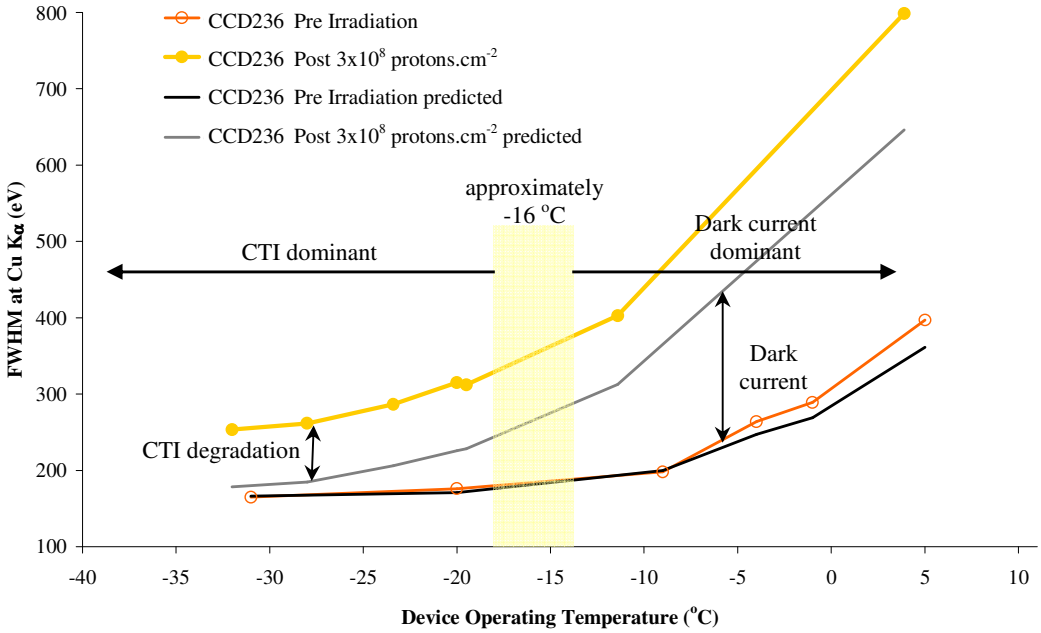

Fig. 9. Measured and predicted (based on noise and Fano factor) energy resolution of isolated Cu-Kα events found using the CCD236 pre and post irradiation as a function of temperature

The increased noise is not enough to account for the decreased energy resolution post irradiation, the radiation induced increase in CTI forms the main component of decreased energy resolution at lower temperatures. The CCD54 in Figure 7 demonstrates that above approximately -6 °C the increased dark current is the dominant source of decreased energy resolution post irradiation, while below increased CTI is dominant. Further cooling bellow -20 °C has little effect on the energy resolution, the performance is CTI limited [Gow and Holland 2009].

The CCD234 in Figure 8 demonstrates that above approximately -12 °C the radiation induced increase in dark current is the dominant source of decreased energy resolution. The reduced impact of increased CTI as a result of proton damage is clear. At -15 °C increased CTI accounts for approximately 78% and 55% of the decrease in energy resolution of ~130 eV and ~90 eV for the CCD54 and CCD234 respectively. The CCD234 also benefits from continued cooling and in the temperature range measured the performance is not yet CTI limited. At around -30 °C the increased CTI accounts for 100% of the decrease in post irradiation energy resolution of ~130 eV and ~50 eV for the CCD54 and CCD234 respectively. It would be expected that due to the lower dark current generated in the CCD234 that the CTI would start to dominate at a higher temperature than in the CCD54. The fact that this is not the case enforces the improved radiation tolerance due to improved charge transfer.

As expected due to its larger active area the CCD236, in Figure 9, demonstrates that above approximately -16 °C the increased dark current is the dominant source of decreased energy resolution post irradiation. At -15 °C increased CTI accounts for approximately 49% of the decrease in post irradiation energy resolution of ~170 eV. As with the CCD234 the device continues to benefit from further cooling, at around -30 °C the increased CTI accounts for approximately 80% of the decrease in energy resolution of ~90 eV. The improved radiation tolerance as a result of reducing the impact of poor CTI is evident below -23 °C where the CCD236 attains a higher energy resolution than the CCD54 despite having four times the active area and dark current.

4. CONCLUSIONS

The next generation SCDs show a clear increase in radiation hardness after receiving a 10 MeV equivalent proton fluence of 3×10^8 protons.cm^{-2}, by around two times that of the CCD54. The measured energy resolution at Cu-Kα is compared in Table 4 at -15 °C and -30 °C for the CCD54, CCD234 and CCD236. The dark current of the CCD54 was comparable with that of the CCD234 pre irradiation, with the dark current generated on the CCD236 being around four times higher due to the four times larger active area. The next generation devices possess a large electrode pitch of 100 µm and a 2-phase clock operation for improved throughput and spectroscopy, compared to the CCD54s 25 µm electrode pitch and 3-phase clock operation, detecting ~70% of Cu-Kα events as isolated compared to the 44% of the CCD54.

The revised pixel structure in the new generation of SCDs gives improved radiation hardness and provides a reduction in the fraction of split events.

Table 4. Energy resolution of isolated Cu-Kα events after receiving a 10 MeV equivalent proton fluence of 3.0×10^8 protons.cm^{-2} and in brackets those values recorded pre irradiation

Temperature (°C)	*CCD54 (eV)*	*CCD234 (eV)*	*CCD236 (eV)*
-15	286 (157)	241 (152)	360 (186)
-30	273 (145)	200 (150)	260 (166)

The increase in noise as a result of radiation induced dark current, believed to be bulk as the surface dark current is suppressed using dither mode clocking. The increase is not sufficient to account for the decrease in measured energy resolution. The remaining loss in performance is as a result of radiation induced increased CTI, the main component of resolution loss at low operating temperatures. The lower temperature dominance of CTI for the next generation devices is a result of the reduced impact of radiation induced increase to the CTI, achieved through changes to the clocking operation and device structure. The slightly higher temperature dependence of the CCD236 is as a result of the devices four times higher dark current due to its four times larger active area.

The CCD234 would allow excellent performance when compared to the CCD54, at -30 °C the CCD234 only suffers a decrease in energy resolution of ~50 eV compared to ~130 eV experienced by the CCD54. The CCD236 allows for four times the readout area with a quarter of the readout electronics, while still able to provide excellent post irradiation performance due to improved radiation hardness. Future work will include a detailed optimisation of the CCD234 and CCD236, measurement and prediction of the CTI effects, explore the slight CTI difference between the CCD234 and CCD236 (possibly due to the additional charge combination structure), and conduct further proton irradiations to different fluence levels with multiple devices for better statistics.

REFERENCES

1. Gow, J., and Holland, A., "CCD234 and CCD236 Preliminary Irradiation Study: Post Irradiation Characterisation and Comparison with CCD54", Open_SCD_TR_002.01 (2009)
2. Gow, J., Smith, D. R., Holland, A. D., Maddison, B., Howe, C., Grande, M., Sreekumar, P., Huovelin, J., "Radiation Study of Swept-Charge Devices for the Chandrayaan-1 X-ray Spectrometer (C1XS) instrument", Proc. SPIE, vol. **7021** (2008)
3. van de Graaf, E., "Flux calibration irradiation for October 28, 2008", Kernfysisch Versneller Instituut dose report (2008)
4. Grande, M., et al., "The D-CIXS X-ray mapping spectrometer on SMART-1", Planetary and Space Science, vol. **51**, pp. 427-433 (2003)
5. Holland, A., "HXMT CCD236 SCD: Initial Test Report", Brunel_HXMT_TR_001.01 (2007)
6. Holland, A., "CCD235/234 SCD: Initial Test Report", Brunel_SCD_TR_001.02 (2007)
7. Howe, C.J., Drummond, D., Edeson, R., Maddison, B., Parker, D.J., Parker, R., Shrivastava, A., Spencer, J., Kellett, B.J., Grande, M., Sreekumar, P., Huovelin, J., Smith, D.R., Gow, J., Narendranath, S. and d'Uston, L., "Chandrayaan-1 X-ray Spectrometer (C1XS) - Instrument design and technical details", Planetary and Space Science, Vol. **57**, Issue 7, pp. 735-743 (2009)